plant biology

Plant Biology ISSN 1435-8603

RESEARCH ARTICLE

Stem and leaf xylem of angiosperm trees experiences minimal embolism in temperate forests during two consecutive summers with moderate drought

X. Guan[1], J. Werner[1], K.-F. Cao[2,3], L. Pereira[1], L. Kaack[1], S. A. M. McAdam[4] & S. Jansen[1]

1 Institute of Systematic Botany and Ecology, Ulm University, Ulm, Germany
2 Plant Ecophysiology and Evolution Group, State Key Laboratory for Conservation and Utilisation of Subtropical Agro-Bioresources, Guangxi University, Nanning, Guangxi, China
3 Guangxi Key Laboratory of Forest Ecology and Conservation, College of Forestry, Guangxi University, Nanning, Guangxi, China
4 Purdue Center for Plant Biology, Department of Botany and Plant Pathology, Purdue University, West Lafayette, IN, USA

Keywords
Hydraulic safety margin; pit characteristics; summer drought; vulnerability segmentation; xylem embolism resistance; xylem anatomy.

Correspondence
X. Guan, Institute of Systematic Botany and Ecology, Ulm University, Albert-Einstein-Allee 11, 89081, Ulm, Germany.
E-mail: xinyi.guan@uni-ulm.de

Editor
N.K. Ruehr

Received: 27 September 2021; Accepted: 2 December 2021

doi:10.1111/plb.13384

ABSTRACT

- Drought events may increase the likelihood that the plant water transport system becomes interrupted by embolism. Yet our knowledge about the temporal frequency of xylem embolism in the field is frequently lacking, as it requires detailed, long-term measurements.
- We measured xylem embolism resistance and midday xylem water potentials during the consecutive summers of 2019 and 2020 to estimate maximum levels of embolism in leaf and stem xylem of ten temperate angiosperm tree species. We also studied vessel and pit membrane characteristics based on light and electron microscopy to corroborate potential differences in embolism resistance between leaves and stems.
- Apart from *A. pseudoplatanus* and *Q. petraea*, eight species experienced minimum xylem water potentials that were close to or below those required to initiate embolism. Water potentials corresponding to ca. 12% loss of hydraulic conductivity (PLC) could occur in six species, while considerable levels of embolism around 50% PLC were limited to *B. pendula* and *C. avellana*. There was a general agreement in embolism resistance between stems and leaves, with leaves being equally or more resistant than stems. Also, xylem embolism resistance was significantly correlated to intervessel pit membrane thickness (T_{PM}) for stems, but not to vessel diameter and total intervessel pit membrane surface area of a vessel.
- Our data indicate that low amounts of embolism occur in most species during moderate summer drought, and that considerable levels of embolism are uncommon. Moreover, our experimental and T_{PM} data show that leaf xylem is generally no more vulnerable than stem xylem.

INTRODUCTION

Water transport along the soil–plant–atmosphere continuum is achieved by a pressure gradient, and this evaporation-driven process frequently occurs under negative pressure (Dixon & Joly 1895). The long-distance transport system in plants can be interrupted by the entry of large bubbles, *i.e.* embolism formation, due to increasing tensile force under drought stress and other largely unknown processes (Tyree & Sperry 1989; Guan *et al.* 2021). The resulting dysfunction of water-conducting conduits decreases hydraulic conductance, transpiration rates and maximum photosynthesis (Zhu *et al.* 2013; Martin-StPaul *et al.* 2017), and may ultimately contribute to the dehydration and death of leaves or branches (Cardoso *et al.* 2020; Powers *et al.* 2020; Nolan *et al.* 2021).

Embolism resistance of plant organs is commonly estimated by constructing vulnerability curves under artificial lab conditions. Water potentials at 12, 50 and 88% loss of hydraulic conductivity (P_{12}, P_{50} and P_{88}) have been used to quantify embolism resistance (Choat *et al.* 2012). A hydraulic safety margin (*HSM*), which can be defined as the difference between minimum xylem water potential (Ψ_{min}) and P_{12} (*i.e.* HSM_{12}) or P_{50} (*i.e.* HSM_{50}), may estimate the probability that a plant faces hydraulic failure and subsequent dehydration under natural field conditions (Meinzer *et al.* 2009; Oliveira *et al.* 2021). Angiosperm species in temperate forests were found to show relatively narrow (<1 MPa) HSM_{50} values, while there could be both inter- and intraspecific variation in embolism resistance and minimum xylem water potential at a local scale (Li *et al.* 2016a; Schuldt *et al.* 2016; Zhang *et al.* 2018; Laughlin *et al.* 2020). Positive *HSM* values could be maintained by the evolution of embolism-resistant xylem (more negative P_{50}) or by controlling Ψ_{min} through low stomatal conductance, leaf shedding and/or developing deep roots (Hochberg *et al.* 2017; Oliveira *et al.* 2021). Moreover, the *HSM* concept has been applied to both stems (Choat *et al.* 2012; Ziegler *et al.* 2019) and leaves (Zhu *et al.* 2016; Yan *et al.* 2020). *HSM* estimations for a large number of species within a vegetation area provide

Plant Biology **24** (2022) 1208–1223 © 2021 The Authors. *Plant Biology* published by John Wiley & Sons Ltd on behalf of German Society for Plant Sciences, Royal Botanical Society of the Netherlands

useful information about the plant water status and potential risk of embolism formation, which can also contribute to drought-induced mortality (Anderegg *et al.* 2016; Powers *et al.* 2020). The potential risk to plants to experiencing xylem embolism in the field could also be important for understanding niche differentiation and species coexistence in a forest (Oliveira *et al.* 2019; Zhang *et al.* 2021).

At the whole-plant level, leaves generally experience the most negative water potential, because they are most exposed to the low water potentials of the atmosphere. Hydraulic segmentation or compartmentalisation, mainly created by resistivity due to the dimensions and arrangement of conduits and bordered pits, drives a water potential gradient between tissues and organs, especially across leaf venations, nodes, growth rings and stem–leaf transitions (Zimmermann 1983; Tyree 1988). The more segmented a plant, the larger the water potential gradient across organs. At the same time, this mechanism may provide protection for organs with high carbon investment, such as branches, trunks and roots, by avoiding low water potentials in those tissues, even when the pressure at the distal leaves is dangerously negative. Hydraulic segmentation is hypothesized to isolate embolism at least temporarily and slow down the process of embolism spread (Zimmermann 1983; Guan *et al.* 2021). The vulnerability segmentation hypothesis becomes especially attractive if xylem in distal organs, such as leaves, were less embolism resistant than stem xylem under drought stress (Tyree & Ewers 1991), with positive vulnerability segmentation ($P_{50\_leaf} > P_{50\_stem}$) acting as a safety valve to protect stems from hydraulic failure (Pivovaroff *et al.* 2014).

Positive vulnerability segmentation has frequently been suggested in the literature (Choat *et al.* 2005; Charrier *et al.* 2016; Johnson *et al.* 2016; Avila *et al.* 2021a), although lack of vulnerability segmentation (Klepsch *et al.* 2018; Skelton *et al.* 2018; Wason *et al.* 2018; Smith-Martin *et al.* 2020) and higher embolism resistance in leaves than in stems has also been observed (Zhu *et al.* 2016, 2019; Klepsch *et al.* 2018; Levionnois *et al.* 2020). While the available evidence seems to suggest that variation in vulnerability segmentation is species-specific, methodological issues related to embolism resistance and measuring artefacts must be considered (Wheeler *et al.* 2013; Torres-Ruiz *et al.* 2015; Lamarque *et al.* 2018). When vulnerability curves are constructed based on hydraulic conductance of leaves, it can be difficult to distinguish loss of conductance in xylem conduits from the outside-xylary pathways, because the conductance of outer-xylary tissues may decrease considerably before embolism occurs in the leaf xylem (Scoffoni *et al.* 2017; Albuquerque *et al.* 2020). This may explain why vulnerability segmentation was reported for temperate forest species by Zhu *et al.* (2016), but not by Li *et al.* (2020).

Embolism resistance refers to the ability to withstand gas entry and embolism spread in the network of plant conduits, and this process can be largely determined by xylem anatomy at the cell wall level (Zimmermann 1983; Lens *et al.* 2011; Kaack *et al.* 2019, 2021). Although major veins, consisting of wide and long vessels, are suggested to embolise prior to small and narrow conduits in minor veins (Brodribb *et al.* 2016b), vessel dimensions may not be directly related to embolism resistance *per se* (Guan *et al.* 2021). Since embolism spread from a gas-filled embolized conduit to a sap-filled conduit involves gas movement through pit membranes (Zimmermann 1983; Sperry & Tyree 1988; Jansen *et al.* 2018; Kaack *et al.* 2019), interconduit pits play a major role in embolism spread. The 'rare pits' hypothesis, which predicts that the probability of leaky pit membranes leading to embolism propagation increases with increasing intervessel pit membrane area per vessel (A_P, mm^2), is frequently assumed to explain why wide and long vessels show relatively low embolism resistance (Wheeler *et al.* 2005; Hacke *et al.* 2006). This hypothesis, however, has been shown to be limited to a fairly narrow range of pit membrane thickness values based on experimental and modelling evidence (*e.g.* Kaack *et al.* 2021; Lemaire *et al.* 2021). Instead of A_P, pit membrane thickness is a highly predictive trait associated with embolism resistance across species, and species with thick intervessel pit membranes typically show strong embolism resistance (Jansen *et al.* 2009; Li *et al.* 2016b; Schuldt *et al.* 2016; Levionnois *et al.* 2021). Pit membrane thickness of leaf xylem, however, has only been measured for a few species, and it remains to be established if pit membrane thickness plays an important role in embolism resistance of leaf veins (Kotowska *et al.* 2020; Zhang *et al.* 2020).

In this study, we measured xylem vulnerability to drought-induced embolism and the *in-situ* water status of stem and leaf xylem in ten temperate deciduous tree species. These measurements allowed us to apply the *HSM* concept, and to estimate the likelihood of embolism occurrence in temperate angiosperm trees during the summers of 2019 and 2020. We hypothesise that positive $HSM_{min\text{-}50}$ values are found in both stems and leaves across the species studied, indicating that high levels of embolism are rare, even during dry summer periods (Cochard & Delzon 2013; Lamarque *et al.* 2018; Dietrich *et al.* 2019). Narrow $HSM_{min\text{-}12}$ values are expected, suggesting these plants may approach the critical threshold to initiate small amounts of embolism. Instead, other processes in the non-xylem pathway, such as stomatal closure, disconnection at the root–soil interface and/or regulation of aquaporins in the root, are likely to take place prior to embolism formation (Vandeleur *et al.* 2009; Carminati & Javaux 2020; Creek *et al.* 2020; Dayer *et al.* 2020; Rodriguez-Dominguez & Brodribb 2020). In addition, we compared the P_{50} values of stem and leaf xylem to evaluate the potential difference in xylem embolism resistance of a given species. We expected leaf xylem to be equally or more vulnerable to embolism than stem xylem because organs with higher carbon investment, such as stems, need to be equally or more protected from hydraulic failure than organs with lower carbon investment. We also examined xylem anatomical traits of leaves and stems, and how these structural characteristics might explain similarity or difference in embolism resistance. Pit characteristics, such as pit membrane thickness, are expected to correlate with embolism resistance, *i.e.* embolism-resistant xylem might have thicker intervessel pit membranes, while conduit dimensions and A_P might not be directly related to P_{50} values.

MATERIAL AND METHODS

Plant material and site information

We studied the following ten temperate angiosperm tree species: *Acer pseudoplatanus*, *Betula pendula*, *Carpinus betulus*, *Corylus avellana*, *Fagus sylvatica*, *Liriodendron tulipifera*, *Prunus avium*, *Quercus petraea*, *Quercus robur* and *Tilia cordata*. All species are found in the forest near Ulm University (Germany,

48°25′20.3″ N, 9°57′20.2″ E) and are common trees in Central European forests, except *L. tulipifera*, which grows at the Botanical Garden of Ulm University. Eight species selected are deciduous and diffuse porous, while the other two are ring-porous species (*Q. petraea* and *Q. robur*).

Climate information at the study site, *i.e.* daily mean temperatures, rainfall, daily maximum vapour pressure deficit (VPD), were obtained from the weather station at Mähringen, Ulm, Germany, which is ca. 2 km from the study site. The meteorological data were accessed from the German Weather Service (https://cdc.dwd.de/portal/). To evaluate the extent of summer drought in 2019 and 2020, we obtained standardized precipitation–evapotranspiration indices (SPEI) of the study site from the Global Drought Monitor platform (https://spei.csic.es). SPEI values were calculated based on a 3-month time resolution, with the calibration period from 1950 to 2010. According to these data, the 2019 and 2020 summers were moderately dry, although the study site had experienced a more extreme drought in 2018.

All measurements were conducted between June and September of 2019 and 2020, except for *B. pendula*, where stem and leaf vulnerability curves were obtained in August 2021. Three trees were selected for each species and one to two branches per tree were sampled. Samples for constructing vulnerability curves were collected from the sun-exposed crown at about 3-m height before 09:00 h. To avoid potential impact of pre-existing embolism due to open vessels (Wheeler *et al.* 2013; Torres-Ruiz *et al.* 2015; Guan *et al.* 2021), long branch samples were first cut in air, and immediately placed in a water-filled bucket. Samples were covered with dark plastic, transferred to the lab within 10 min, kept in water for >2 h for rehydration, then recut under water by removing a ca. 20 cm stem segment (Wheeler *et al.* 2013). The length of the remaining branch samples was 80–160 cm, which is longer than the maximum vessel length in stem xylem (L_{V_max}).

Embolism resistance of leaf xylem

Leaf vulnerability curves (*VC*) were constructed using the optical method of Brodribb *et al.* (2016a,b). A healthy, mature and undamaged leaf from each sampled branch (80–160 cm length) was fixed under a stereomicroscope (Axio Zoom.V16; Zeiss, Jena, Germany), or in optical clamps (http://www.opensourceov.org/), and ca.1 cm^2 leaf area photographed every 5 min. The water potential was simultaneously monitored on a healthy leaf near the sampled leaf or on stem xylem of the same branch using a psychrometer (PSY1; ICT International, Armidale, NSW, Australia) at 15-min intervals. For leaf *VC*, PSY1 was used for leaves of all species, except *Tilia cordata*. The PSY1 was attached to stem xylem of *T. cordata* because of mucilage secretion from leaves of this species. Leaf water potential was also measured regularly on different leaves of the same branch using a pressure chamber (PMS Instrument Co., Albany, OR, USA) to validate the psychrometer data. Leaves from at least four branches of different individuals were used to capture embolism events and to construct leaf xylem vulnerability curves. Leaf vulnerability curves of *C. betulus*, *F. sylvatica*, *L. tulipifera*, *P. avium* and *Q. petraea* were retrieved from Guan *et al.* (2021).

Images were processed using the OpenSourceOV ImageJ Toolbox with the Fiji version of ImageJ (Schindelin *et al.* 2012). When embolism formation occurred in leaf xylem, the brightness of the leaf veins changed, and the time elapsed and quantity of these events were evaluated by stacking the optical images. The percentage total embolized pixels (PEP) was quantified over time at decreasing leaf xylem water potentials, with P_{50} representing the xylem water potential corresponding to 50% total embolized pixels (Brodribb *et al.* 2016a).

Embolism resistance of stem xylem

A ChinaTron flow centrifuge (Model H2100R; Xiangyi, China) was used to construct vulnerability curves for the eight diffuse-porous tree species. After sample preparation, stem segments of 27.4-cm length were excised under water, with both ends trimmed and debarked. Stems were mounted in the centrifuge rotor with their ends in cuvettes, and spun at 2000 rpm, corresponding to a water potential of −0.25 MPa, to determine maximum hydraulic conductivity (K_{max}). The tension was increased stepwise, and the hydraulic conductivity (K_h) was measured after 5 min once the set rotation speed had been reached. Measurements ended at percentage loss of conductivity (PLC) >98%, or when PLC no longer increased with increasing centrifuge speed. The PLC at each tension was calculated as:

$$PLC = 100 \times (K_{max} - K_h)/K_{max}$$

The tension generated in the ChinaTron was converted to xylem water potential by subtracting atmospheric pressure of 0.1 MPa from the total pressure generated in the centre of the centrifuge. The relationship between PEP/PLC and xylem water potential was plotted for stem and leaf xylem. Vulnerability curves were fitted with a sigmoid equation (Pammenter & Van der Willigen 1998). P_{12}, P_{50} and P_{88} (MPa) were extracted from the vulnerability curves, with P_{x_stem} corresponding to xylem water potential at x% loss of maximum hydraulic conductivity/total embolism event and P_{x_leaf} corresponding to water potential at x% of total embolism events in xylem of leaf veins.

Stem vulnerability curves of *Q. petraea* and *Q. robur* were constructed using the optical method as their maximum vessel length was much longer than the rotor length of the ChinaTron centrifuge (Wang *et al.* 2014). Stem vulnerability curves of *B. pendula* were constructed with both the ChinaTron centrifuge and the optical method to test whether P_{50} values obtained using the two methods were similar. The overall agreement of *VC*s based on the two methods has been confirmed for various species (Brodribb *et al.* 2017; Lamarque *et al.* 2018; Sergent *et al.* 2020). The length of terminal branch samples for these three species was ca. 1.2 m, which was longer than the maximum vessel length of the stem xylem (L_{V_max}; Table S1). We applied the optical method to stem material with a diameter < 0.5 cm (Brodribb *et al.* 2017). Stem psychrometers were applied to the stem ca. 50 cm from both the cut end of the branch and the observed terminal branchlet. After gently removing the bark, a psychrometer was carefully attached to the exposed xylem, held in place with a clamp and sealed with Vaseline to prevent changes in humidity. Since all stem psychrometer measurements were conducted under controlled lab conditions, diurnal temperature changes were minimal. Images of the stem xylem area and water potential measurements were taken every 15 min. Similar to measurement of leaves, we regularly checked

water potential results of the psychrometers against results obtained with a pressure chamber.

Midday water potentials

Midday water potentials (Ψ_{md}, MPa) were measured with a pressure chamber between 12:00 h and 14:00 h on sunny days during summer of 2019 and 2020. Measurements were taken on the same individuals used to construct vulnerability curves, to avoid intraspecific variation. To determine water potentials of stem xylem, one branchlet of two to three individuals per species was covered with aluminium foil on the evening before measurements were taken to allow equilibration of the water potential between stems and bagged leaves. Midday water potentials of leaves were determined based on unbagged, transpiring leaves. After collection at midday, leaves were immediately placed into plastic bags containing moist tissue, while avoiding direct contact of the moist tissue with the leaves. The leaves were stored in a foam box in darkness and brought back to the laboratory within 1 h. The non-transpiring leaf water potential measurements represent stem water potential (Ψ_{md_stem}), while the transpiring leaf water potential measurements represent leaf water potential (Ψ_{md_leaf}). We conducted measurements over 12 days, carefully selected based on local weather forecasts for Ulm. Hence, the 12 measurement days typically represent the driest days at the end of a rainless period (usually 1 to 2 weeks; see Fig. 1). The most negative water potentials (Ψ_{min}) for each species were selected to indicate water status of different organs during summer drought. Although we carefully selected the driest days over two consecutive summers, we are aware that minimum water potential measurement days may have been missed.

Hydraulic safety margins

Hydraulic safety margins (*HSM*) were calculated as: $HSM_{min\text{-}12}$ and $HSM_{min\text{-}50}$ referring to the difference between Ψ_{min} and P_{12} ($\Psi_{min} - P_{12}$) and Ψ_{min} and P_{50} ($\Psi_{min} - P_{50}$), respectively.

The degree of stem–leaf vulnerability segmentation, defined as $P_{50\_leaf} - P_{50\_stem}$, was also calculated. Positive segmentation refers to leaves being more vulnerable than stems. We also compared the degree of vulnerability segmentation in this study with results of other published embolism resistance data that focused on xylem tissue (Levionnois *et al.* 2020; Li *et al.* 2020).

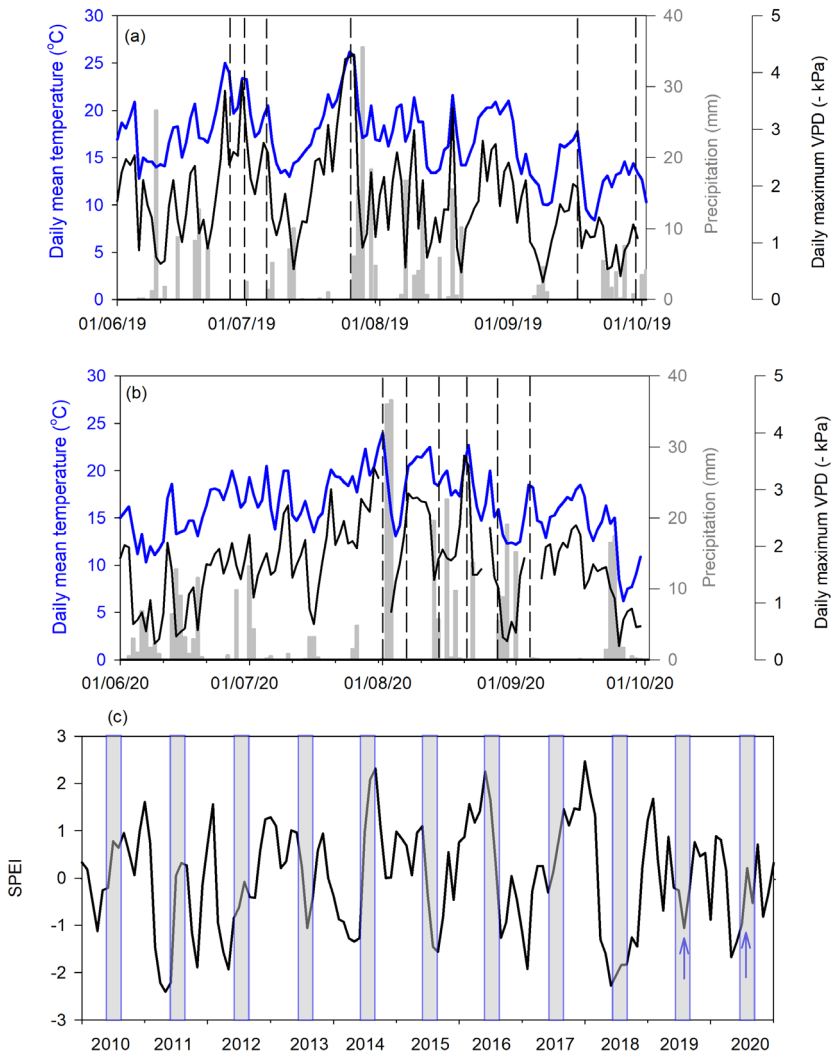

Fig. 1. Daily variations in mean temperature (°C, blue line), precipitation (mm, grey bars) and maximum vapour pressure deficit (VPD, kPa, black line) during summer 2019 (a) and 2020 (b). Black vertical dashes indicated dates when midday water potentials were measured. Climate data from Mähringen, Ulm, ca. 2 km from the field site, were obtained from the German weather Service (https://cdc.dwd.de/portal/) (c). Variation in the standardized precipitation evapotranspiration index (SPEI) based on average of 3-month periods between 2010 and 2020, showing moderate drought in 2019 and 2020, following a more severe drought in 2018. Grey boxes are summer (June to September) and blue arrows highlight summers of 2019 and 2020.

Anatomical traits

Terminal branch samples were taken from the same individuals used to determine xylem embolism resistance. To obtain sufficient variation, we sampled one stem segment and one leaf midrib from each individual, with three individuals per species. Only one sample was prepared for transmission electronic microscopy (TEM) due to the time-consuming nature of this method. A list of the traits measured, together with definitions and abbreviations, can be found in Table 1.

Table 1. List of acronyms of characters used in this study, with reference to their definitions and units.

acronym	definition	unit
Ψ_{min_leaf} and Ψ_{min_stem}	Minimum (*i.e.* most negative) xylem water potential measured at midday for leaf and stem xylem in 2019 and 2020	MPa
P_{12}, P_{50}, P_{88}	Water potential at 12%, 50% and 88% of the total embolism events or loss of hydraulic conductivity	MPa
$HSM_{min\text{-}12\_leaf}$ and $HSM_{min\text{-}50\_leaf}$	Leaf hydraulic safety margin based on the minimum xylem water potential and P_{12}/P_{50}, $= \Psi_{min} - P_{12}$ or $\Psi_{min} - P_{50}$	MPa
$HSM_{min\text{-}12\_stem}$, and $HSM_{min\text{-}50\_stem}$	Stem hydraulic safety margin based on minimum xylem water potential and P_{12}/P_{50}, $= \Psi_{min} - P_{12}$ or $\Psi_{min} - P_{50}$	MPa
V_D	Vessel density, number of vessels per mm^2	no. mm^{-2}
V_G	Vessel-grouping index, total number of vessels divided by number of vessel groups; a solitary vessel counts as one vessel group	/
D	Equivalent circle diameter of vessels	μm
L_{V_max}	Maximum vessel length based on air-injection method	cm
L_V	Average vessel length based on vessel length distribution data	cm
A_{pit}	Intervessel pit surface area, pit area occupied by the pit border or intervessel pit membrane	μm^2
F_{PF}	Pit-field fraction, fraction of intervessel wall area occupied by intervessel pits	/
F_C	Intervessel contact fraction, fraction of vessel wall in contact with other vessels based on transverse sections	
F_P	Pit fraction, fraction of total vessel wall area occupied by intervessel pits, $= F_C \times F_{PF}$	/
A_P	Total pit membrane surface area for a vessel with average diameter and length, $= \pi \times D \times L_v \times F_P$	mm^2
T_{PM_centre}, T_{PM_edge}, $T_{PM\_average}$	Thickness of an intervessel pit membrane at the centre, near the edges, and mean value of both areas based on transmission electron microscopy	nm

Scanning electron microscopy (SEM)

Segments 0.5-cm long were cut and split tangentially. After drying at room temperature overnight, samples were mounted on stubs and sputter-coated with gold using a Balzers Union FL-9496 sputter device (Balzers, Liechtenstein). Observations were taken with a Phenom XL SEM (Phenom-World, Eindhoven, the Netherlands) at an acceleration voltage of 10 kV. Special attention was paid to distinguish interconduit pits from conduit-parenchyma pits. Pit membrane surface area (A_{pit}, μm^2) was measured and pit-field fraction (F_{PF}) defined as the fraction of intervessel wall area occupied by intervessel pits.

Light and transmission electron microscopy

Fresh xylem samples of stems and leaves were cut into small segments of ca. 1 mm × 1 mm × 2 mm and fixed with a standard fixation solution (2.5% glutaraldehyde, 0.1 M phosphate, 1% sucrose, pH 7.3) overnight. After washing in 0.2 M phosphate buffer, samples were postfixed with buffered 2% OsO_4 solution, gradually dehydrated in a propanol series (30%, 50%, 70%, 90% and 100%), then stained *en bloc* with a saturated solution of uranyl acetate in ethanol. Samples were immersed in 1.2-propylene oxide and gradually embedded in Epon resin (Sigma-Aldrich, Steinheim, Germany), which was polymerized at 60°C for 48 h. Transverse, semi-thin sections (ca. 500-nm thick) were cut with an ultramicrotome (Leica Ultracut UCT; Leica Microsystems, Vienna, Austria), stained with 0.5% toluidine blue in 0.1 M phosphate buffer, and mounted on microscope slides using Eukitt® (Sigma-Aldrich).

Conduit characteristics of branch and midrib xylem were measured on semi-thin, transverse sections under a light microscope (Zeiss Axio Scope. A1). Arithmetic mean vessel diameter (D, μm) was measured based on more than 50 vessels per sample from sections of three individuals per species. The intervessel contact fraction (F_C) was calculated as the ratio of the sum of the intervessel contact length to the sum of the total vessel perimeter. We also measured a vessel grouping index (V_G), defined as the total number of vessels divided by the total number of vessel groups including solitary and grouped vessels as well as vessel density (V_D, number per mm^2).

Ultra-thin sections (70–90-nm thick) were made with an ultramicrotome (Leica Microsystems) and placed on copper grids (300 mesh per inch; Plano, Wetzlar, Germany). Only focused on xylem of recent growth rings in stems as well as whole xylem area in leaf midribs. TEM observations were conducted using a JEOL 1400 TEM (JEOL, Tokyo, Japan) at a 120 kV accelerating voltage, and images were taken with a digital camera (Soft Imaging System, Münster, Germany). For each sample, at least 20 clearly identifiable interconduit pit membranes were imaged. Pit membrane thickness was measured both near the centre (T_{PM_centre}) and at edges (T_{PM_edge}), where $T_{PM\_average}$ refers to average of T_{PM_centre} and T_{PM_edge}.

All image analyses were conducted with the Fiji version of ImageJ (Schindelin *et al.* 2012).

Vessel length determination

Maximum vessel length of stems and leaf petioles was determined using the air injection method (Greenidge, 1952). We used a syringe to apply ca. 150 kPa pressure to the basipetal part of a stem or petiole and successively cut the proximal end under water until the first continuous stream of air bubbles could be seen emerging from the cut end. The corresponding

length was then measured and recorded as maximum vessel length (L_{V_max}) of a stem or leaf petiole. For each species, more than four stems or leaves of different individuals were taken for L_{V_max} measurements.

The vessel length distribution in stems and leaf petioles was measured with a Pneumatron device (Pereira *et al.* 2020) on more than four stems and leaves per species. The air conductivity of cut and open vessels was plotted against the segment length and fitted to the equations of Sperry *et al.* (2005) to calculate average vessel length (L_V). This method has been validated against the silicon-injection method (Cohen *et al.* 2003; Pan *et al.* 2015; Pereira *et al.* 2020). Vessel length distribution data of leaf petioles of *B. pendula*, *C. betulus*, *F. sylvatica*, *L. tulipifera* and *Q. petraea* were retrieved from Guan *et al.* (2021)

By combining anatomical results from LM, SEM and vessel length determinations, we calculated the total pit membrane surface area for a vessel with an average diameter and length (A_P, mm^2) as $A_P = F_C \times F_{PF} \times \pi \times D \times L_V$ (Wheeler *et al.* 2005). A_p values could not be obtained for stems of the two *Quercus* species because of insufficient intervessel walls to estimate F_C. Also, L_V could not be measured in leaves of *T. cordata* due to mucilage secretion from cut leaves.

Statistics and data analysis

Vulnerability curves were plotted and fitted in SigmaPlot 14.0 (Systat Software, Erkrath, Germany). After testing data for normal distribution and homogeneity of variance, we applied an independent sample *t*-test to check for differences between leaf and stem xylem embolism resistance. We also calculated the root mean square deviation (RMSD) between P_{50} values of stem and leaf xylem: $RMSD = \sqrt{\sum \frac{(P50_{leaf} - P50_{stem})^2}{n}}$.

Pearson's correlation analysis was applied to determine the relationship between anatomical traits and embolism resistance, and a principal components analysis (PCA) was performed in R (http://CRAN-R-project.org) to examine the extent of leaf xylem differences from those of stem xylem, after examining significance of Bartlett's test for sphericity, and testing the suitability of our data for factor analysis, based on Kaiser–Meyer–Olkin values (KMO) of > 0.55.

RESULTS

Meteorological data during summer 2019 and 2020

The average daily air temperature varied from 10 to 25°C. Rainfall mainly occurred in June and August, but July had little precipitation in both 2019 and 2020 (Fig. 1a and b). SPEI values of the summer period (from June to August) in 2019 and 2020 were −1.06 and −1.36, respectively (Fig. 1c), which corresponds to moderate drought (Paulo *et al.* 2012).

Water potential measurements and turgor loss point

We observed a large intraspecific variation in Ψ_{md} of stem and leaf xylem during the consecutive summers of 2019 and 2020, which was affected by canopy transpiration because of changes in air temperature and precipitation (Fig. 1, Figure S2). Ψ_{min} also varied among species, *i.e. P. avium* showed the most negative Ψ_{min} at −2.65 MPa for stem xylem and −2.73 MPa for leaf xylem, while *A. pseudoplatanus* showed comparatively higher values of Ψ_{min}, with −1.00 MPa and −1.03 MPa for stem and leaf xylem, respectively. Leaf Ψ_{min} was more negative than stem Ψ_{min} for most species, except *B. pendula*, *C. betulus* and *Q. petraea*, in which the two values converged (Table 2). Published

Table 2. Key hydraulic traits of stem and leaf xylem for the ten studied temperate deciduous species.

species	organ	P_{12}	P_{50}	P_{88}	Ψ_{min}	HSM_{min-12}	HSM_{min-50}
Acer pseudoplatanus	Stem	−2.49 ± 0.14	−3.19 ± 0.10	−3.89 ± 0.16	−1.00	1.49	2.29
	Leaf	−2.94 ± 0.29	−3.27 ± 0.47	−3.61 ± 0.66	−1.03	1.91	2.24
Betula pendula	Stem	−1.71 ± 0.22	−1.96 ± 0.18	−2.21 ± 0.15	−1.88	**−0.17**	0.08
	Leaf	−2.00 ± 0.11	−2.16 ± 0.16	−2.31 ± 0.22	−1.83	0.17	0.33
Carpinus betulus	Stem	−2.25 ± 0.46	**−3.35 ± 0.41**	−4.46 ± 0.47	−2.05	0.20	1.30
	Leaf	−4.45 ± 0.88	**−4.87 ± 0.81**	−5.28 ± 0.82	−2.00	2.45	2.87
Corylus avellana	Stem	−1.53 ± 0.09	**−1.80 ± 0.11**	−2.08 ± 0.14	−1.9	**−0.37**	**−0.1**
	Leaf	−2.41 ± 0.06	**−2.68 ± 0.19**	−2.95 ± 0.33	−2.03	0.36	0.55
Fagus sylvatica	Stem	−2.40 ± 0.06	**−3.05 ± 0.12**	−3.69 ± 0.22	−2.05	0.35	1.00
	Leaf	−3.46 ± 0.46	**−3.94 ± 0.43**	−4.37 ± 0.53	−2.35	1.11	1.59
Liriodendron tulipifera	Stem	−1.52 ± 0.09	−1.78 ± 0.11	−2.05 ± 0.15	−1.20	0.32	0.58
	Leaf	−1.89 ± 0.87	−2.46 ± 0.71	−3.03 ± 0.65	−1.30	0.69	1.16
Prunus avium	Stem	−2.96 ± 0.21	**−3.69 ± 0.09**	−4.42 ± 0.24	−2.65	0.31	1.04
	Leaf	−3.08 ± 1.25	**−5.53 ± 0.44**	−7.81 ± 1.14	−2.73	0.35	2.8
Quercus petraea	Stem	−3.60 ± 0.70	−4.34 ± 0.57	−5.08 ± 0.54	−1.65	1.95	2.69
	Leaf	−3.90 ± 0.28	−5.07 ± 0.15	−6.24 ± 0.15	−1.62	2.28	3.45
Quercus robur	Stem	−2.35 ± 0.30	−3.10 ± 0.39	−3.85 ± 0.49	−2.35	0	0.75
	Leaf	−2.87 ± 0.15	−3.41 ± 0.21	−3.94 ± 0.31	−2.35	0.52	1.06
Tilia cordata	Stem	−2.07 ± 0.10	**−2.75 ± 0.05**	−3.43 ± 0.06	−1.93	0.14	1.22
	Leaf	−1.98 ± 0.23	**−2.22 ± 0.17**	−2.46 ± 0.13	−2.00	**−0.02**	0.22

Ψ_{min} values were based on *in situ* water potential measurements. Values indicate mean ± SD (n = 4 or 5 for P_{12}, P_{50} and P_{88}).
Significant difference between stem and leaf xylem based on an independent sample *t*-test ($P < 0.05$). P_{12}, P_{50} and P_{88} of leaf for *C. betulus*, *F. sylvatica*, *L. tulipifera*, *P. avium* and *Q. petraea* were retrieved from Guan *et al.* (2021). Acronyms are given in Table 1. Bold indicates negative values.

data on the xylem water potential corresponding to turgor loss of leaves (Ψ_{tlp}) provided an additional criterion to estimate the water status that the plants experienced in the field (Table S2). Values of Ψ_{min} were more negative than the mean Ψ_{tlp} for *P. avium*, and the difference between Ψ_{min} and Ψ_{tlp} ($\Psi_{min} - \Psi_{tlp}$) was less than 0.2 MPa for six species, but much higher for *A. pseudoplatanus*, *C. betulus* and *Q. petraea* (Table S2).

Xylem embolism resistance

The P_{50_leaf} varied from −2.16 to −5.53 MPa across the sampled species, with *B. pendula* having the most vulnerable and *P. avium* the most resistant leaf xylem (Fig. 2, Table 2). Values of P_{50_stem} varied from −1.78 MPa for *L. tulipifera* to −4.34 MPa for *Q. petraea*. (Fig. 2, Table 2). No difference was found between P_{50_stem} obtained with both the ChinaTron and the optical method for *B. pendula* (Figure S3), therefore P_{50_stem} values of *B. pendula* obtained by the optical method were used in all statistical analyses.

The P_{50_leaf} was significantly correlated with P_{50_stem} ($R^2 = 0.72$, $P < 0.01$) for all ten study species (Fig. 3a). Leaf xylem was more embolism-resistant than stem xylem in four species, namely *C. betulus*, *C. avellana*, *F. sylvatica* and *P. avium*, while *T. cordata* showed slightly positive vulnerability segmentation ($P_{50\_stem} < P_{50\_leaf}$). No significant differences between leaf and stem xylem embolism resistance were found in the other five species, namely *A. pseudoplatanus*, *B. pendula*, *L. tulipifera*, *Q. petraea* and *Q. robur* (Fig. 3a, Table 2).

Hydraulic safety margins

The $HSM_{min\text{-}12}$ ranged from −0.02 to 2.45 MPa for leaf xylem, and from −0.17 to 1.95 MPa for stem xylem. *A. pseudoplatanus* and *Q. petraea* showed wide safety margins, with values for leaves and stems above 1.4 MPa for $HSM_{min\text{-}12}$. Negative $HSM_{min\text{-}12}$ values were recorded for *B. pendula*, *C. avellana* and *T. cordata*, while the remaining five species had slightly positive values, suggesting that the most minimum water potentials experienced in the field during the driest periods were slightly higher (*i.e.* less negative) than the P_{12} values (Table 2).

The $HSM_{min\text{-}50}$ ranged from 0.22 to 3.45 MPa for leaf xylem and from −0.1 to 2.69 MPa for stem xylem. *Q. petraea* had the largest $HSM_{min\text{-}50}$ in both stem and leaf xylem. *B. pendula* and *C. avellana* had negative *HSM* in stem xylem but not in leaves, indicating that 30% to 70% of vessels in stems may have been embolized during the driest period of the two summers (Table 2, Fig. 2). $HSM_{min\text{-}50}$ values of leaves were also positively related to stem $HSM_{min\text{-}50}$ ($R^2 = 0.54$, $P = 0.01$; Fig. 3b).

Xylem anatomy

Pearson's correlations between the anatomical characteristics and xylem embolism resistance (P_{50}) were calculated (Table 3). At the vessel level, P_{50} was not significantly related to vessel diameter (D) or average vessel length (L_V) when stem and leaf xylem were considered together. Moreover, no significant correlation between P_{50} and D was found when stem and leaf xylem were analysed separately (Fig. 4d). P_{50} was negatively correlated with average vessel length L_V ($r = -0.641$, $P = 0.046$) for stem xylem, indicating that stems with longer vessels had more negative P_{50} values, but this was not found in leaf xylem. Stem P_{50} decreased with decreasing vessel density V_D ($r = 0.665$, $P = 0.036$) for stem xylem, but no observations were conducted on vessel density for leaves because the vessels grouped in vascular bundles of leaves had an extremely high vessel density (Table 3). No significant relationship was found between P_{50} of stems and vessel grouping index (V_G).

Pit membrane thickness varied widely, from 200 to 500 μm in stem and leaf xylem. A narrower range in *Ap* was found for leaves than for stems (Figure S1, Fig. 4a and b) because values of the pit surface area (A_{pit}), vessel diameter (D) and average vessel length (L_V) of leaf xylem were generally smaller than those of stem xylem (Table S1). There was a significant correlation between $T_{PM\_average}$ and P_{50} ($r = -0.766$, $P = 0.010$) for stem xylem, such that species with thicker intervessel pit membranes tended to have higher embolism resistance. A significant correlation was also found between T_{PM_centre} and P_{50} ($r = -0.789$, $P = 0.007$), as well as between T_{PM_edge} and P_{50} ($r = -0.757$, $P = 0.011$) for stem xylem. Embolism resistance of leaf xylem increased with increasing thickness of pit membranes, but there was no significant relationship between T_{PM_centre} and P_{50} ($r = -0.615$, $P = 0.058$). Two outliers in this relationship were *C. betulus* and *Q. petraea*, which showed strong embolism resistance (P_{50} values around −5 MPa) for a rather moderate pit membrane thickness (ca. 250–300 nm; Fig. 4a). There was a significant correlation between T_{PM_centre}, $T_{PM\_average}$, T_{PM_edge} and P_{50} when pooling stem and leaf xylem data (Table 3). Pit membrane traits, which refer to the size, area and density of intervessel pit membranes, such as A_{pit}, F_{PF} and A_P, were not related to xylem embolism resistance in stem or leaf xylem (Table 3, Fig. 4b).

There was a strong correlation between vessel diameter (D) and average vessel length (L_V) at both the stem and leaf level across all species (Fig. 4c). The ring-porous species *Q. petraea* and *Q. robur* had much longer and wider vessels in stem xylem compared to the diffuse porous species, but variation in vessel dimensions of leaf xylem was rather narrow (Fig. 4c, Table S1). T_{PM_centre} was positively related to vessel diameter (D), average vessel length (L_V) and maximum vessel length (L_{V_max}) when analysing both stem and leaf xylem data together (Figures S5 and S6). Significant correlations between T_{PM_centre} and these parameters were only found for stem xylem data, not for leaf xylem (Figure S6). As such, wide and long vessels in the stem xylem appeared to have thicker intervessel pit membranes than the narrow, short vessels. However, this relationship was strongly affected by the long and wide vessels in the stem xylem of the two *Quercus* species, which had thick intervessel pit membranes of around 500 nm in their stem xylem (Figures S1 and S5).

A PCA for the ten traits of both stem and leaf xylem showed that the first two principal components explained 43.6% and 22.6% of the total variation, respectively (Fig. 5a). The first PC was mainly produced by quantitative pit characteristics, such as F_{PF} (30.87%), A_{pit} (27.92%) and A_P (22.78%; Fig. 5c). The second PC was largely explained by traits related to the safety of hydraulic transport in the xylem, such as P_{50} (39.68%), followed by Ψ_{min} and T_{PM_centre} (30.22% and 18.08%, respectively; Fig. 4d). There was more interspecific variation in stem xylem than in leaf xylem on the first principal axis, but similar

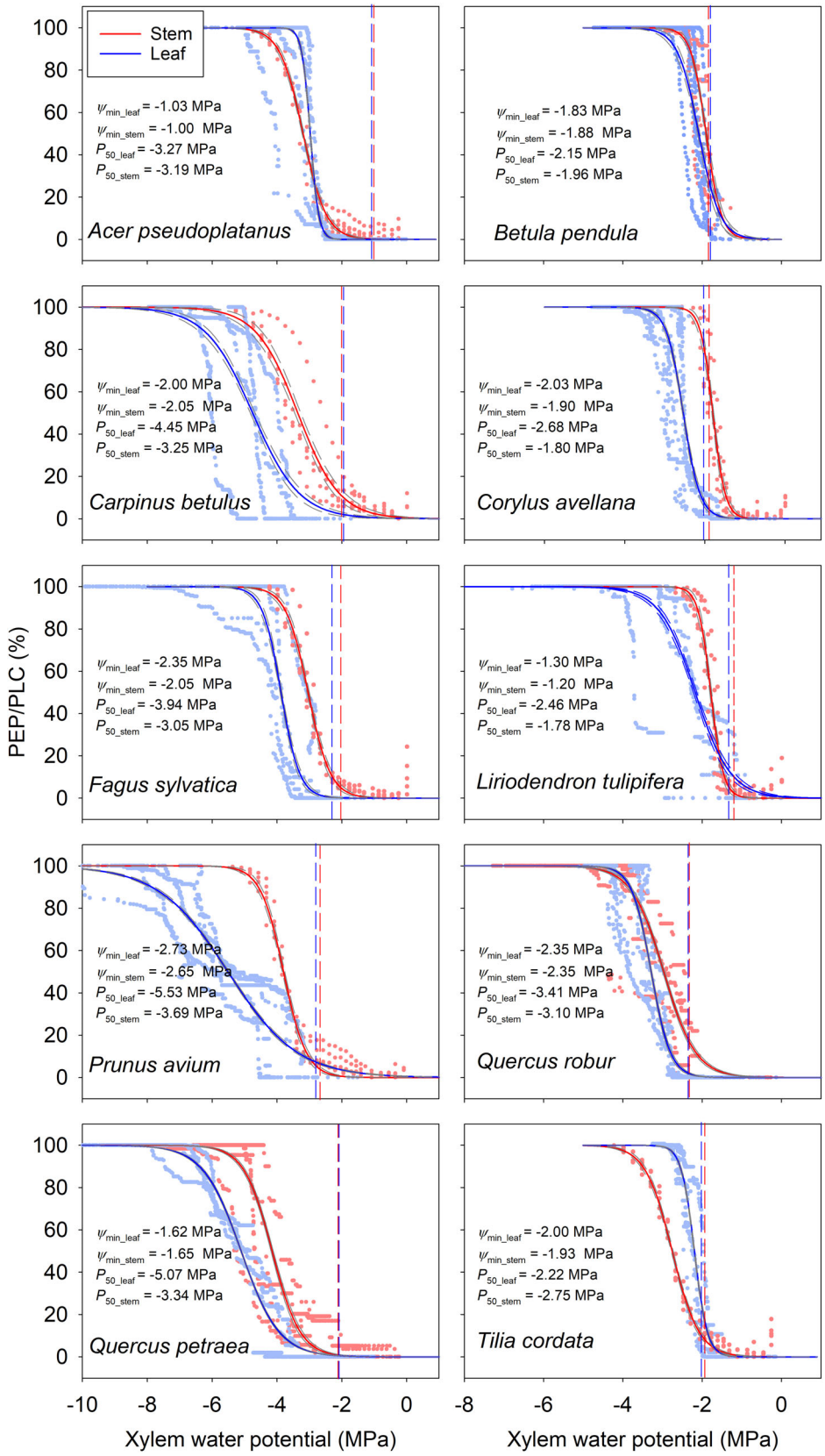

Fig. 2. Vulnerability curves for leaf (blue) and stem (red) xylem of ten deciduous angiosperm species. Four to five specimens were measured (dots in light colours) for each species. Solid lines are curve fittings and grey lines indicate 95% confidence intervals. Vertical dashed lines indicate most negative xylem water potentials (Ψ_{min}) measured during summers of 2019 and 2020.

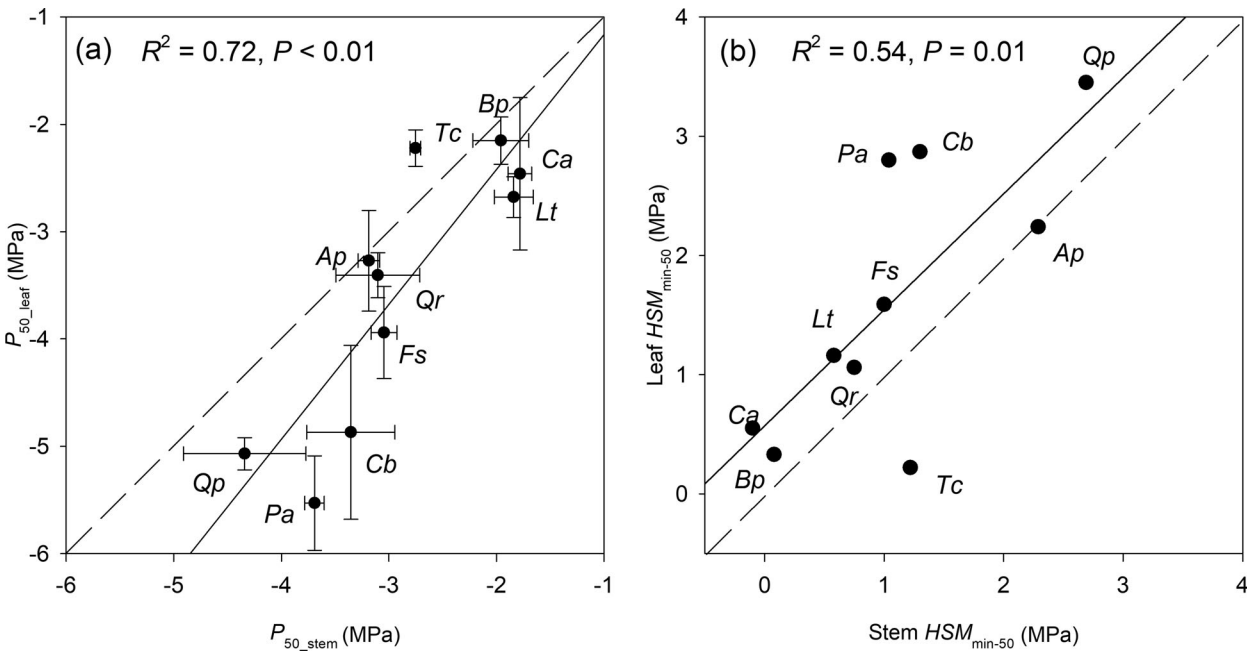

Fig. 3. (a) Water potential at 50% loss of conductance or embolism events in stem xylem (P_{50_stem}) plotted against water potential at 50% embolism events in leaf xylem (P_{50_leaf}). (b) Leaf xylem hydraulic safety margin (Leaf HSM_{min-50}) against stem xylem hydraulic safety margin (Stem HSM_{min-50}). Dots represent mean of xylem embolism resistance of species studied in (a) and (b), with bi-directional error bars showing ±SD in (a). Solid line indicates linear regression line, and dashed line indicates 1:1 line. Ap = *Acer pseudoplatanus*, Bp = *Betula pendula*, Ca = *Corylus avellana*, Cb = *Carpinus betulus*, Fs = *Fagus sylvatica*, Lt = *Liriodendron tulipifera*, Pa = *Prunus avium*, Qp = *Quercus petraea*, Qr = *Quercus robur* and Tc = *Tilia cordata*.

Table 3. Pearson correlations for relationships between P_{50} and xylem anatomical characteristics.

		stem and leaf P_{50}		stem P_{50}		leaf P_{50}	
	anatomical traits	*r*	*P*-value	*r*	*P*-value	*r*	*P*-value
Vessel Level	D	0.018	0.941	−0.383	0.275	0.136	0.707
	L_V	−0.127	0.603	**−0.641**	**0.046**	−0.005	0.999
	V_D	/	/	**0.665**	**0.036**	/	/
	V_G	/	/	0.323	0.363	/	/
Pit level	$T_{PM\_average}$	**−0.581**	**0.007**	**−0.766**	**0.010**	−0.605	0.064
	T_{PM_centre}	**−0.595**	**0.006**	**−0.789**	**0.007**	−0.615	0.058
	T_{PM_edge}	**−0.577**	**0.008**	**−0.757**	**0.011**	−0.578	0.080
	A_{pit}	−0.010	0.968	−0.302	0.397	−0.306	0.390
	A_P	0.118	0.651	−0.542	0.166	−0.006	0.988
	F_C	−0.169	0.503	0.312	0.452	−0.081	0.825
	F_{PF}	0.202	0.393	−0.146	0.686	0.000	0.999

Values in bold indicate a significant (P < 0.05) correlation. All acronyms are according to Table 1.

variation in stem and leaf xylem was found along the second principal axis. (Fig. 5b).

DISCUSSION

The positive HSM_{min-50} values of both stem and leaf xylem indicate that almost all of the ten tree species studied had a low likelihood of considerable amounts of embolism (*i.e.* >50% PLC) forming in the field during dry summer days of 2019 and 2020. This finding highlights the temporal frequency of embolism occurrence in the field, suggesting that considerable embolism is rare during moderately dry summers. Two exceptions to this general finding were stem xylem of *B. pendula* and *C. avellana* (see below). The most negative xylem water potentials experienced were close to P_{12}, or even slightly below this threshold of embolism initiation, for eight out of the ten species studied. Moreover, our results provide no evidence that leaf xylem is significantly more vulnerable to embolism formation than stem xylem in nine out of the ten species studied. While pit membrane thickness was related to embolism resistance in stem xylem, its functional correlation for leaf xylem was only marginally significant. Apart from pit membrane thickness, no other anatomical trait measured at the conduit and pit level was correlated with P_{50}. The broader significance of these findings is discussed below.

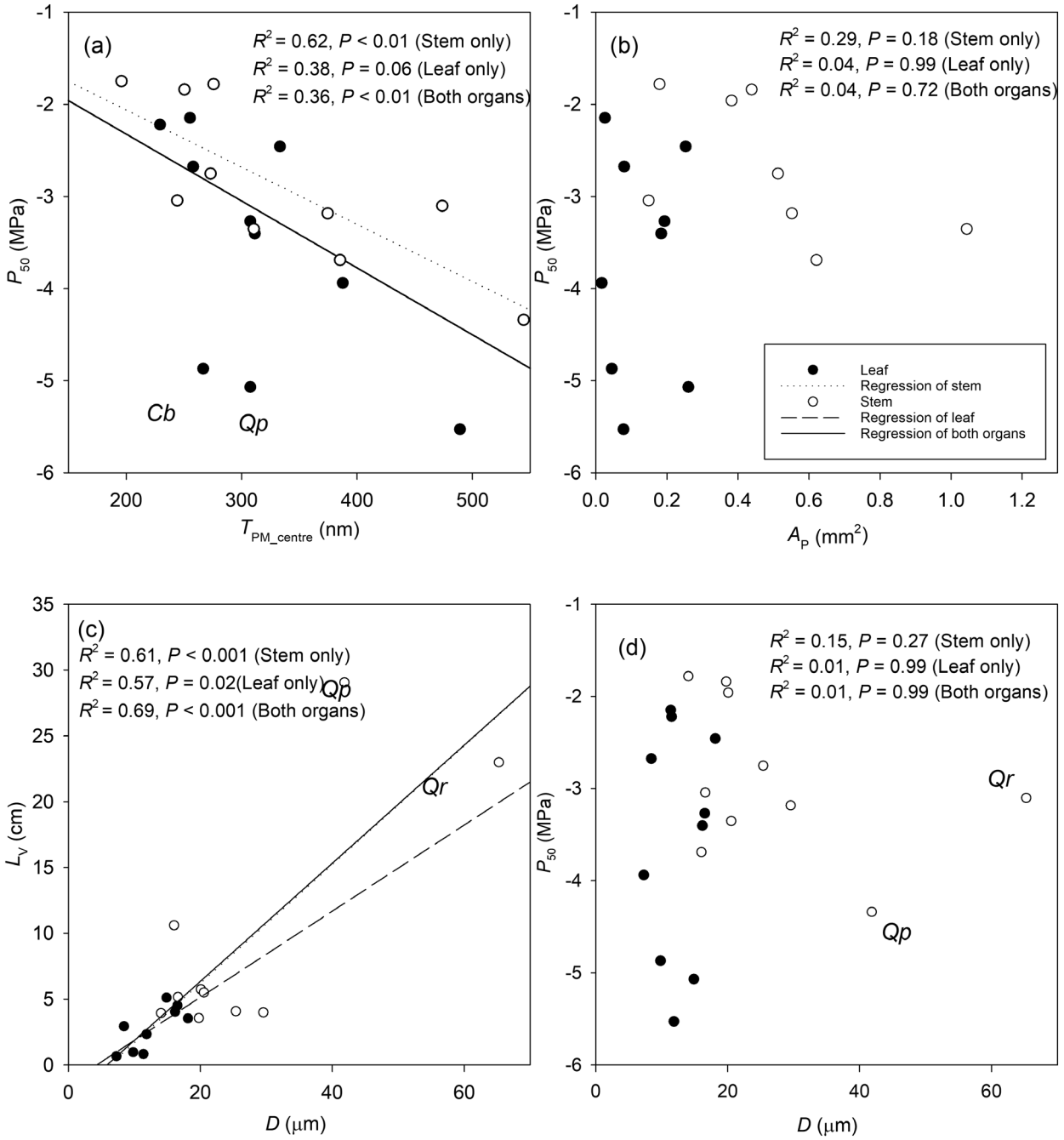

Fig. 4. Relationship of (a) xylem embolism resistance (P_{50}) and central pit membrane thickness (T_{PM_centre}), (b) P_{50} and average interconduit pit membrane area per vessel (A_P), (c) mean vessel length (L_V) and vessel diameter (D), and (d) P_{50} and vessel diameter (D) in both stem xylem (circles) and leaf xylem (dots) for the ten studied temperate tree species.

There is a low risk of high levels of drought-induced embolism in stem and leaf xylem

Negative $HSM_{min\text{-}12}$ values were recorded for three species (*B. pendula*, *C. avellana* and *T. cordata*), and positive, but narrow (<0.5 MPa) $HSM_{min\text{-}12}$ values were found in five other species. Therefore, the $HSM_{min\text{-}12}$ values indicated that low levels of embolism, well below 50% PLC, may occur in six out of the ten tree species studied, although around 50% PLC could occur in *B. pendula* and *C. avellana*. Embolism, however, is very unlikely to occur in *A. pseudoplatanus* and *Q. petraea* (Fig. 2, Table 2). At the stem level, Dietrich *et al.* (2019) found wide and positive $HSM_{min\text{-}50}$, with values around 2 MPa in six common temperate species during a severe drought in 2015, demonstrating that the stem hydraulic system was far from dysfunctional during periods of severe drought. However, *HSM* may vary among species, site and season. Schuldt *et al.* (2020), for instance, reported negative $HSM_{min\text{-}12}$ values in one third of the native tree populations in Central Europe during a severe drought in 2018, which suggests that at least some

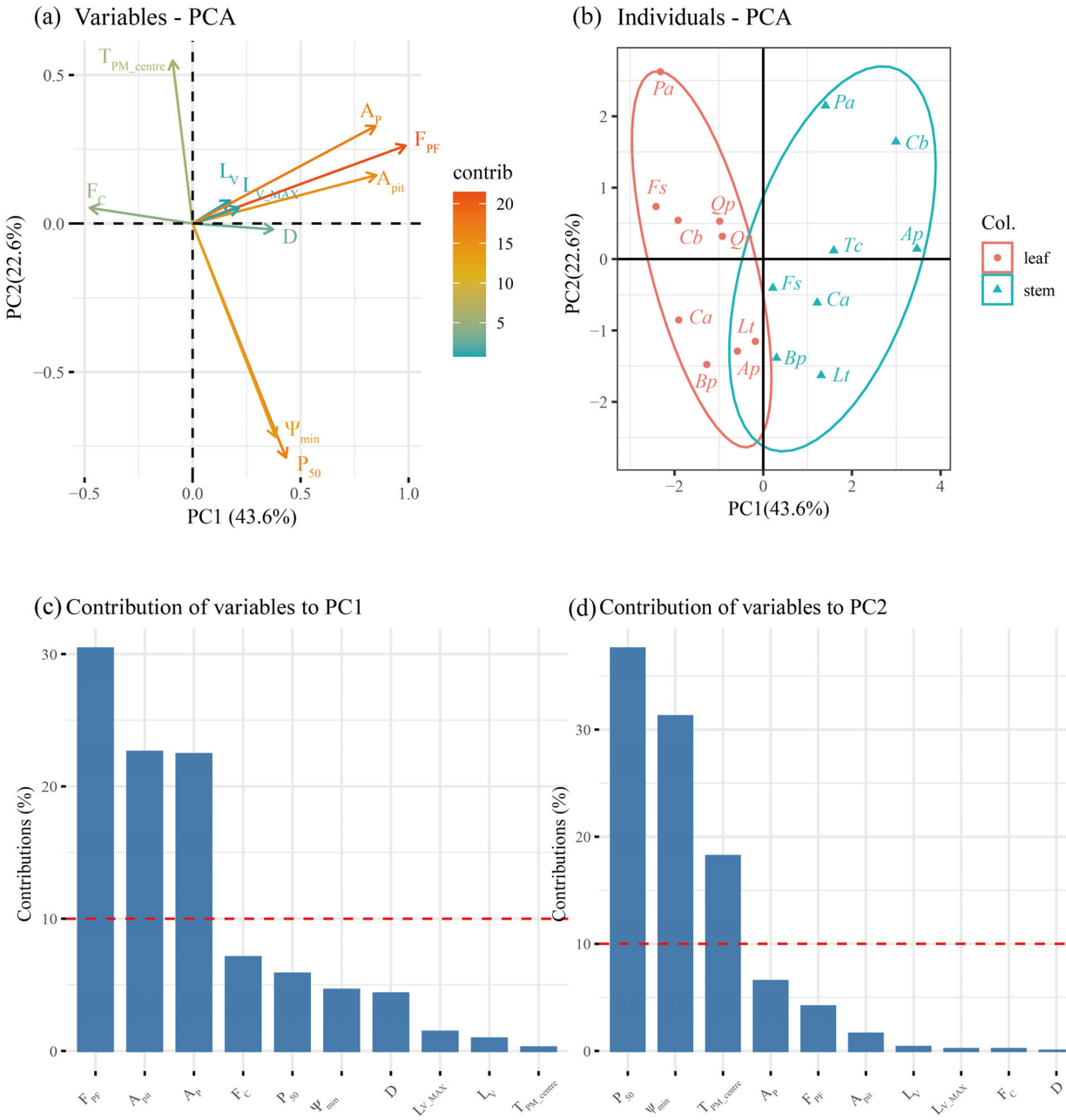

Fig. 5. Principal components analysis (PCA) of anatomical characteristics and hydraulic traits for both leaf and stem xylem of ten tree species. (a) Loading of first two principal components (PC), and (b) scores for each species along PC1 and PC2 based on leaf xylem (red circles) and stem xylem (blue triangles). Percentage variance explained by the first two PCs is shown on axis labels. (c and d) Contribution of variables to the first and second PC, respectively ranked from high to low. Red dashed lines in (c) and (d) indicate average contribution of each variable.

conduits would be embolized. The SPEI for the summer of 2018 was less than −2, indicating an extreme drought event, while the SPEI values of the summers of 2019 and 2020 represent moderate drought (Fig. 1). Although we recognize that the absolute lowest water potentials during the summers of 2019 and 2020 could have been missed due to the lack of a long-term and high temporal resolution to monitor water potentials directly, our Ψ_{min} and *HSM* data provide a meaningful estimate of embolism occurrence in the trees studied. Moreover, when plants experience an SPEI of −2, it is possible that other physiological barriers respond in a non-linear way, *e.g.* water potential at the root–soil interface may drop extremely rapidly to negative values after reaching a critical threshold (Carminati & Javaux 2020). Similarly, embolism risk under extreme drought could become exponentially higher than that under moderate drought.

Our results differ from the narrow hydraulic safety margins of stem xylem for temperate forest angiosperms (n = 67 species) found by Choat *et al.* (2012), which contained $HSM_{min\text{-}50}$ values from −1.49 to 3.15 MPa, with a median of 0.42 MPa. However, embolism resistance of 18 out of 67 species from this dataset might have been underestimated

because of their exponential vulnerability curves, which are now generally thought to reflect measuring artefacts (Wheeler *et al.* 2013; Jansen *et al.* 2015; Torres-Ruiz *et al.* 2017; Lamarque *et al.* 2018). Besides, leaf instead of stem Ψ_{min} was measured in most cases, which could have led Choat *et al.* (2012) to overestimate the likelihood of xylem embolism occurrence.

Why do the vulnerability curves and Ψ_{min} values suggest that considerable levels of embolism occur in stem xylem of *B. pendula* and *C. avellana* during the driest summer periods? This question is difficult to explain as there was no obvious dieback of leaves or branches in either species. The Ψ_{min} values and vulnerability curves obtained indicated that 30% to 70% of the vessels would have embolized in stems of both species (Fig. 2). Since our P_{50_stem} values for these two species are similar to the P_{50_stem} data for plants from the same population based on earlier studies using different methods (including bench dehydration, pneumatic measurements and the flow-centrifuge method; Li *et al.* 2016a; Zhang *et al.* 2018; Kaack *et al.* 2021), it is unlikely that our measurements underestimated the embolism resistance. It is possible that minor shifts in embolism resistance of *B. pendula* and *C. avellana* (ca. 0.5 MPa) occurred during the growing season (unpublished data). Embolism resistance has been found to shift with osmotic adjustment during soil drought in sunflower (Cardoso *et al.* 2018) and in grapevine (Sorek *et al.* 2021) as the growing season progresses. Another alternative is that *B. pendula* had a brief period of positive xylem pressure before leaf flush during early spring (Hölttä *et al.* 2018; Guan *et al.*, unpublished data), which could refill embolized vessels in the stem xylem (Hao *et al.* 2013; Schenk *et al.* 2021). However, the likelihood of refilling occurring in the summer to maintain hydrated leaves has little support. A final possibility is that there could be a considerable degree of hydraulic redundancy in the stem of these Betulaceae species, which would allow some embolism to occur but without a sufficient loss of stem hydraulic conductivity to lower leaf water potentials. These possibilities all require future investigation.

While relatively few studies have focused on leaf *HSM* in temperate forests, narrow and even negative HSM_{50} has been found in leaves of most temperate species (Johnson *et al.* 2016; Yan *et al.* 2020; Avila *et al.* 2021a). The overall large and positive HSM_{50} of leaf xylem for the ten temperate trees in our study suggests that leaf xylem of temperate angiosperms does not experience a high risk of considerable embolism formation. Negative HSM_{50} could be largely related to stomatal closure and/or dysfunction of the outer xylem tissue instead of xylem embolism formation where vulnerability curves were constructed based on hydraulic measurements of the whole leaf (Scoffoni *et al.* 2017).

Stem xylem is not more resistant to embolism than leaf xylem in the studied species

Our data show that leaf xylem can be significantly less (*T. cordata*), significantly more (*C. betulus*, *C. avellana*, *F. sylvatica*, *P. avium*) or equally (*A. pseudoplatanus*, *B. pendula*, *L. tulipifera*, *Q. petraea*, *Q. robur*) resistant to embolism compared with stem xylem (Fig. 3, Table 2). The RMSD, which reflects the difference between two sets of data, shows a 0.98 MPa difference between P_{50} values of stem and leaf xylem in this study. Since two different methods were applied to these two organs, RMSD values could be due to this methodological difference. An RMSD value of 0.73 MPa was found for stem segments tested with the optical and flow-centrifuge method (Fig. 4 in Brodribb *et al.* 2017). However, vulnerability curves of stem and leaf xylem of *B. pendula* were constructed simultaneously on the same branch using the optical method in August 2021, and a *post-hoc* test suggested that here was no significant difference between stem P_{50} measured with the ChinaTron or with the optical method (Figure S3). Comparison of P_{50_stem} and P_{50_leaf} with previously published values for all species showed a similar pattern: embolism resistance was higher, similar or lower for leaves than for stems (Figure S4). The variation in P_{50} values between both organs is consistent with similar results from a tropical rainforest (Levionnois *et al.* 2020) and for other temperate species (Avila *et al.* 2021a), and demonstrates that species growing under the same climate conditions may have different vulnerability segmentation strategies, which are integrated with other physiological traits to cope with drought stress.

Tilia cordata is the only species in which leaf xylem appeared slightly more vulnerable to embolism than stem xylem. Because *T. cordata* contains mucilage in leaves, leaf water potential measurements with a pressure chamber or a psychrometer were challenging, but it was possible to successfully monitor water potential using a stem psychrometer mounted on a branch. Moreover, we assumed similar water potentials in leaf and stem after stomatal closure (Rodriguez-Dominguez *et al.* 2018; Avila *et al.* 2021a) as this species is strongly isohydric, with sensitive stomatal regulation, and can maintain a rather constant minimum water potential (Leuschner *et al.* 2019).

Five species showed no vulnerability segmentation (Table 2). *L. tulipifera* had similar embolism resistance in leaves and branches, as reported in other studies (Klepsch *et al.* 2018; Li *et al.* 2020), and there was good agreement in P_{50} values for *Q. robur* and *Q. petraea* with other oak species (Skelton *et al.* 2018). P_{50} values for leaf and stem xylem of *B. pendula* are in line with those of Li *et al.* (2020) and may be common in the genus *Betula*, as similar results have been observed in *B. pubescens* (Avila *et al.* 2021a).

Four out of the ten species studied showed a higher embolism resistance for leaf xylem than for stem xylem (Table 2, Fig. 3a). One of these species was *F. sylvatica*, for which there was no difference in P_{50} values between stem (−2.74 MPa) and major leaf veins (−2.26 MPa) of seedlings, based on micro-CT (Losso *et al.* 2019). It is unclear whether the ratio in xylem embolism resistance between leaf and stem xylem remains consistent between seedlings and mature, adult trees. Also, major veins of leaves are known to embolise prior to secondary and other higher order veins (Brodribb *et al.* 2016a,b; Guan *et al.* 2021). Hence, leaf xylem embolism resistance could be underestimated if observations are limited to major veins. Our results largely agree with findings that tropical species have more vulnerable stems than leaves and show rather strong embolism resistance (Levionnois *et al.* 2020), with neither xylem in leaves nor in stems being vulnerable to embolism in the field. Finally, the finding that leaves of some species are more embolism resistant than stems does not automatically imply that embolism occurrence in stem xylem is more likely because leaves may experience more negative xylem water potentials than stems. As such, the likelihood of embolism in stem xylem and

leaf xylem may be similar in the field, despite differences in their relative embolism resistance. The fact that the T_{PM} of leaf xylem is not less than that of stem xylem, provides additional, anatomical support for equal or higher embolism resistance in leaf xylem than in stem xylem.

Pit membrane thickness predicts embolism resistance of stem xylem

Species with thick intervessel pit membranes typically present high xylem embolism resistance, is in agreement with studies at both intra- and interspecific level (Lens *et al.* 2011; Li *et al.* 2016b; Schuldt *et al.* 2016; Levionnois *et al.* 2021). Interestingly, this well-known relationship was marginally significant ($r = -0.616$, $P = 0.058$; Fig. 4a) for primary xylem in leaves of our study species. The lack of a strong relationship between pit membrane thickness and embolism resistance in leaf xylem was also found by Levionnois *et al.* (submitted) for 18 tropical rainforest species. It is unclear to what extent our results can be generalized, but current evidence suggests that pit membrane thickness in leaves is only weakly associated with embolism resistance of leaf xylem. Recently, Kaack *et al.* (2021) provided a functional explanation for why pit membrane thickness is associated with embolism resistance. These authors suggested that movement of gas (both mass flow and diffusion) across a pit membrane is largely determined by the size of the narrowest pore constriction within the pit membrane, which is strongly affected by the number of cellulose microfibril layers. Since pit membrane thickness likely reflects the number of microfibril layers, and thus the number of pore constrictions, increasing pit membrane thickness would probably lead to a higher chance of having a narrow pore constriction (Kaack *et al.* 2019, 2021).

We found no relationship between xylem embolism resistance and total pit membrane area per vessel with the average length and diameter (A_P) in neither stem nor leaf xylem (Fig. 4b), as was proposed by the rare pit hypothesis (Wheeler *et al.* 2005; Hacke *et al.* 2006). A_p may explain the relatively limited variation in P_{50} between poplar individuals (Lemaire *et al.* 2021), but *A*p affects P_{50} in a different way to T_{PM}, which may even uncouple hydraulic safety from efficiency (Kaack *et al.* 2021). While *A*p might have a minor effect on P_{50} over a rather narrow range of T_{PM}, T_{PM} is clearly a much stronger determinant of P_{50} than *A*p (Kaack *et al.* 2021).

Although conduit length scaled less with conduit diameter in leaf than in stem xylem, the average vessel length (L_V) was significantly correlated with vessel diameter (D) in both organs. Hence, a long vessel usually had a large diameter (Fig. 4c), consistent with previous studies (Hacke *et al.* 2006; Cai *et al.* 2010; Olson & Rosell 2013; Liu *et al.* 2018). Moreover, leaf midribs usually embolized before secondary and higher order veins, but there was no relationship between vessel diameter and embolism resistance among the species studied (Fig. 4d), as also reported by Avila *et al.* (2021a). Embolism spread may also depend on the connection of conduits with pre-existing embolism (Avila *et al.* 2021a; Guan *et al.* 2021). The xylem network connectivity between stem and leaf xylem, however, remains to be studied in more detail for more species in order to better understand how vessel dimensions and connectivity contribute to embolism propagation (Avila *et al.* 2021b; Mrad *et al.* 2021; Wason *et al.* 2021).

ACKNOWLEDGEMENTS

We thank Andrea Huppenberger and Clara Garcia Sanchez for lab assistance, colleagues from the botanical garden for assistance with sampling plant material, and the Electron Microscopy Section of Ulm University for technical support with TEM. XG, K.-F.C and SJ acknowledge financial support from the Deutsche Forschungsgemeinschaft (project 410768178). K.-F.C acknowledges financial support from the National Natural Science Foundation of China (grant no. 31861133008). SM was supported by a fellowship from the Alexander von Humboldt Foundation. We thank anonymous reviewers for their helpful comments and suggestions.

SUPPORTING INFORMATION

Additional supporting information may be found online in the Supporting Information section at the end of the article.

Table S1. Xylem anatomical traits related to (a) vessel and (b) pit characteristics of a stem and leaf midrib for ten species. Acronyms of characters are given in Table 1 and values indicate mean ± standard deviation. / = no data could be obtained.

Table S2. Overview of water potential at turgor loss point (Ψ_{tlp}, MPa) for the species studied based on literature. $\Psi_{min} - \Psi_{tlp}$ values indicate the difference of Ψ_{min} and mean Ψ_{min}.

Figure S1. Light microscopy (LM) images of xylem cross-sections and transmission electron microscopy (TEM) images of interconduit pit membranes in *Corylus avellana* (a, c, e and g) and *Quercus petraea* (b, arrows in d, f and h). a–d represent branch xylem and e–f include leaf xylem. Scale bars: 100 μm for LM images and 2 μm for TEM images.

Figure S2. Variations of midday xylem water potentials during the summer of 2019 (a) and 2020 (b). Each species was represented by a symbol with different colours and the dashed line indicates the 1:1 line.

Figure S3. Vulnerability curves of stem xylem for *Betula pendula*. The three sets of points (red circles, red triangles and red filled triangles) and fitted curves (red dashed, red solid and black dashed lines) represent xylem vulnerability curves obtained with a flow-centrifuge (CE) in August 2019, a flow-centrifuge in August 2021, and the optical method (OV) in August 2021, respectively.

Figure S4. Comparison of stem and leaf P_{50} values, and leaf values that focussed on xylem only were considered. Grey circles represent data from Li *et al.* (2020) and Levionnois *et al.* (2020), and black circles were species measured in this study. The dashed line indicates the 1:1 line and the solid line indicates linear regression based on the P_{50} value pairs measured in this study.

Figure S5. Pearson's correlation coefficients for all pairwise trait comparisons based on ten species. Coefficient values for significant correlations ($P < 0.05$) are shown, which is reflected in the shape and direction of the ellipses, while a blank background means that there is no significant coefficient.

Figure S6. Relationship of T_{PM_centre} and D (a), L_{V_max} (b) and L_V (c) for stem and leaf xylem studied. Stem data are shown in white circles, and leaf data in black triangles. Coefficients of determination and statistical significance are shown, and linear regressions are shown when the relationship is significant ($P < 0.05$).

REFERENCES

Albuquerque C., Scoffoni C., Brodersen C.R., Buckley T.N., Sack L., McElrone A.J. (2020) Coordinated decline of leaf hydraulic and stomatal conductances under drought is not linked to leaf xylem embolism for different grapevine cultivars. *Journal of Experimental Botany*, **71**, 7286–7300.

Anderegg W.R., Klein T., Bartlett M., Sack L., Pellegrini A.F., Choat B., Jansen S. (2016) Meta-analysis reveals that hydraulic traits explain cross-species patterns of drought-induced tree mortality across the globe. *Proceedings of the National Academy of Science*, **113**, 5024–5029.

Avila R.T., Cardoso A.A., Batz T.A., Kane C.N., DaMatta F.M., McAdam S.A. (2021a) Limited plasticity in embolism resistance in response to light in leaves and stems in species with considerable vulnerability segmentation. *Physiologia Plantarum*, **172**, 2142–2152.

Avila R., Guan X., Kane C., Cardoso A., Batz T., DaMatta F., Jansen S., McAdam S. (2021b) Xylem embolism spread is largely prevented by interconduit pit membranes until the majority of conduits are gas-filled. *Authorea Preprints*. https://doi.org/10.22541/au.162864525.54313554/v1

Brodribb T.J., Bienaimé D., Marmottant P. (2016b) Revealing catastrophic failure of leaf networks under stress. *Proceedings of the National Academy of Sciences*, **113**, 4865–4869.

Brodribb T.J., Carriqui M., Delzon S., Lucani C. (2017) Optical measurement of stem xylem vulnerability. *Plant Physiology*, **174**, 2054–2061.

Brodribb T.J., Skelton R.P., McAdam S.A., Bienaimé D., Lucani C.J., Marmottant P. (2016a) Visual quantification of embolism reveals leaf vulnerability to hydraulic failure. *New Phytologist*, **209**, 1403–1409.

Cai J., Zhang S., Tyree M.T. (2010) A computational algorithm addressing how vessel length might depend on vessel diameter. *Plant, Cell & Environment*, **33**, 1234–1238.

Cardoso A.A., Batz T.A., McAdam S.A. (2020) Xylem embolism resistance determines leaf mortality during drought in *Persea americana*. *Plant Physiology*, **182**, 547–554.

Cardoso A.A., Brodribb T.J., Lucani C.J., DaMatta F.M., McAdam S.A. (2018) Coordinated plasticity maintains hydraulic safety in sunflower leaves. *Plant, Cell & Environment*, **41**, 2567–2576.

Carminati A., Javaux M. (2020) Soil rather than xylem vulnerability controls stomatal response to drought. *Trends in Plant Science*, **25**, 868–880.

Charrier G., Torres-Ruiz J.M., Badel E., Burlett R., Choat B., Cochard H., Delmas C.E.L., Domec J.-C., Jansen S., King A., Lenoir N., Martin-StPaul N., Gambetta G.A., Delzon S. (2016) Evidence for hydraulic vulnerability segmentation and lack of xylem refilling under tension. *Plant Physiology*, **172**, 1657–1668.

Choat B., Jansen S., Brodribb T.J., Cochard H., Delzon S., Bhaskar R., Bucci S.J., Feild T.S., Gleason S.M., Hacke U.G., Jacobsen A.L., Lens F., Maherali H., Martínez-Vilalta J., Mayr S., Mencuccini M., Mitchell P.J., Nardini A., Pittermann J., Pratt R.B., Sperry J.S., Westoby M., Wright I.J., Zanne A.E. (2012) Global convergence in the vulnerability of forests to drought. *Nature*, **491**, 752–755.

Choat B., Lahr E.C., Melcher P.J., Zwieniecki M.A., Holbrook N.M. (2005) The spatial pattern of air seeding thresholds in mature sugar maple trees. *Plant, Cell & Environment*, **28**, 1082–1089.

Cochard H., Delzon S. (2013) Hydraulic failure and repair are not routine in trees. *Annals of Forest Science*, **70**, 659–661.

Cohen S., Bennink J., Tyree M. (2003) Air method measurements of apple vessel length distributions with improved apparatus and theory. *Journal of Experimental Botany*, **54**, 1889–1897.

Creek D., Lamarque L.J., Torres-Ruiz J.M., Parise C., Burlett R., Tissue D.T., Delzon S. (2020) Xylem embolism in leaves does not occur with open stomata: evidence from direct observations using the optical visualization technique. *Journal of Experimental Botany*, **71**, 1151–1159.

Dayer S., Herrera J.C., Dai Z., Burlett R., Lamarque L.J., Delzon S., Bortolami G., Cochard H., Gambetta G.A. (2020) The sequence and thresholds of leaf hydraulic traits underlying grapevine varietal differences in drought tolerance. *Journal of Experimental Botany*, **71**, 4333–4344.

Dietrich L., Delzon S., Hoch G., Kahmen A. (2019) No role for xylem embolism or carbohydrate shortage in temperate trees during the severe 2015 drought. *Journal of Ecology*, **107**, 334–349.

Dixon H.H., Joly J. (1895) On the ascent of sap. *Philosophical Transactions of the Royal Society of London B, Biological Sciences*, **186**, 563–576.

Greenidge K.N.H. (1952) An approach to the study of vessel length in hardwood species. *American Journal of Botany*, **39**, 570–574.

Guan X., Pereira L., McAdam S.A., Cao K.F., Jansen S. (2021) No gas source, no problem: Proximity to pre-existing embolism and segmentation affect embolism spreading in angiosperm xylem by gas diffusion. *Plant, Cell & Environment*, **44**, 1329–1345.

Hacke U.G., Sperry J.S., Wheeler J.K., Castro L. (2006) Scaling of angiosperm xylem structure with safety and efficiency. *Tree Physiology*, **26**, 689–701.

Hao G.Y., Wheeler J.K., Holbrook N.M., Goldstein G. (2013) Investigating xylem embolism formation, refilling and water storage in tree trunks using frequency domain reflectometry. *Journal of Experimental Botany*, **64**, 2321–2332.

Hochberg U., Windt C.W., Ponomarenko A., Zhang Y.J., Gersony J., Rockwell F.E., Holbrook N.M. (2017) Stomatal closure, basal leaf embolism, and shedding protect the hydraulic integrity of grape stems. *Plant Physiology*, **174**, 764–775.

Hölttä T., Dominguez Carrasco M.D.R., Salmon Y., Aalto J., Vanhatalo A., Bäck J., Lintunen A. (2018) Water relations in silver birch during springtime: How is sap pressurised? *Plant Biology*, **20**, 834–847.

Jansen S., Choat B., Pletsers A. (2009) Morphological variation of intervessel pit membranes and implications to xylem function in angiosperms. *American Journal of Botany*, **96**, 409–419.

Jansen S., Klepsch M., Li S., Kotowska M.M., Schiele S., Zhang Y., Schenk H.J. (2018) Challenges in understanding air-seeding in angiosperm xylem. *Acta Horticulturae*, **1222**, 13–20.

Jansen S., Schuldt B., Choat B. (2015) Current controversies and challenges in applying plant hydraulic techniques. *New Phytologist*, **205**, 961–964.

Johnson D.M., Wortemann R., McCulloh K.A., Jordan-Meille L., Ward E., Warren J.M., Palmroth S., Domec J.-C. (2016) A test of the hydraulic vulnerability segmentation hypothesis in angiosperm and conifer tree species. *Tree Physiology*, **36**, 983–993.

Kaack L., Altaner C.M., Carmesin C., Diaz A., Holler M., Kranz C., Neusser G., Odstrcil M., Jochen Schenk H., Schmidt V., Weber M., Zhang Y.A., Jansen S. (2019) Function and three-dimensional structure of intervessel pit membranes in angiosperms: a review. *IAWA Journal*, **40**, 673–702.

Kaack L., Weber M., Isasa E., Karimi Z., Li S., Pereira L., Trabi C.L., Zhang Y.A., Schenk H.J., Schuldt B., Schmidt V., Jansen S. (2021) Pore constrictions in intervessel pit membranes provide a mechanistic explanation for xylem embolism resistance in angiosperms. *New Phytologist*, **230**, 1829–1843.

Klepsch M., Zhang Y.A., Kotowska M.M., Lamarque L.J., Nolf M., Schuldt B., Torres-Ruiz J.M., Qin D.-W., Choat B., Delzon S., Scoffoni C., Cao K.-F., Jansen S. (2018) Is xylem of angiosperm leaves less resistant to embolism than branches? Insights from microCT, hydraulics, and anatomy. *Journal of Experimental Botany*, **69**, 5611–5623.

Kotowska M.M., Thom R., Zhang Y., Schenk H.J., Jansen S. (2020) Within-tree variability and sample storage effects of bordered pit membranes in xylem of *Acer pseudoplatanus*. *Trees*, **34**, 61–71.

Lamarque L.J., Corso D., Torres-Ruiz J.M., Badel E., Brodribb T.J., Burlett R., Charrier G., Choat B., Cochard H., Gambetta G.A., Jansen S., King A., Lenoir N., Martin-StPaul N., Steppe K., Van den Bulcke J., Zhang Y.A., Delzon S. (2018) An inconvenient truth about xylem resistance to embolism in the model species for refilling *Laurus nobilis* L. *Annals of Forest Science*, **75**, 1–15.

Laughlin D.C., Delzon S., Clearwater M.J., Bellingham P.J., McGlone M.S., Richardson S.J. (2020) Climatic limits of temperate rainforest tree species are explained by xylem embolism resistance among angiosperms but not among conifers. *New Phytologist*, **226**, 727–740.

Lemaire C., Brunel-Michac N., Santini J., Berti L., Cartailler J., Conchon P., Badel E., Herbette S. (2021) Plasticity of the xylem vulnerability to embolism in *Populus tremula x alba* relies on pit quantity properties rather than on pit structure. *Tree Physiology*, **41**, 1384–1399.

Lens F., Sperry J.S., Christman M.A., Choat B., Rabaey D., Jansen S. (2011) Testing hypotheses that link wood anatomy to cavitation resistance and hydraulic conductivity in the genus *Acer*. *New Phytologist*, **190**, 709–723.

Leuschner C., Wedde P., Lübbe T. (2019) The relation between pressure–volume curve traits and stomatal regulation of water potential in five temperate broadleaf tree species. *Annals of Forest Science*, **76**, 1–14.

Levionnois S., Jansen S., Wandji R.T., Beauchêne J., Ziegler C., Coste S., Stahl C., Delzon S., Authier L., Heuret P. (2021) Linking drought-induced xylem embolism resistance to wood anatomical traits in Neotropical trees. *New Phytologist*, **229**, 1453–1466.

Levionnois S., Ziegler C., Jansen S., Calvet E., Coste S., Stahl C., Salmon C., Delzon S., Guichard C., Heuret P. (2020) Vulnerability and hydraulic segmentations at the stem–leaf transition: coordination across Neotropical trees. *New Phytologist*, **228**, 512–524.

Li S., Feifel M., Karimi Z., Schuldt B., Choat B., Jansen S. (2016a) Leaf gas exchange performance and the lethal water potential of five European species during drought. *Tree Physiology*, **36**, 179–192.

Li S., Lens F., Espino S., Karimi Z., Klepsch M., Schenk H.J., Schmitt M., Schuldt B., Jansen S. (2016b)

Intervessel pit membrane thickness as a key determinant of embolism resistance in angiosperm xylem. *IAWA Journal*, **37**, 152–171.

Li X., Delzon S., Torres-Ruiz J., Badel E., Burlett R., Cochard H., Jansen S., King A., Lamarque L.J., Lenoir N., St-Paul N.M., Choat B. (2020) Lack of vulnerability segmentation in four angiosperm tree species: evidence from direct X-ray microtomography observation. *Annals of Forest Science*, **77**, 1–12.

Liu M., Pan R., Tyree M.T. (2018) Intra-specific relationship between vessel length and vessel diameter of four species with long-to-short species-average vessel lengths: further validation of the computation algorithm. *Trees*, **32**, 51–60.

Losso A., Bär A., Dämon B., Dullin C., Ganthaler A., Petruzzellis F., Savi T., Tromba G., Nardini A., Mayr S., Beikircher B. (2019) Insights from in vivo micro-CT analysis: testing the hydraulic vulnerability segmentation in *Acer pseudoplatanus* and *Fagus sylvatica* seedlings. *New Phytologist*, **221**, 1831–1842.

Martin-StPaul N., Delzon S., Cochard H. (2017) Plant resistance to drought depends on timely stomatal closure. *Ecology Letters*, **20**, 1437–1447.

Meinzer F.C., Johnson D.M., Lachenbruch B., McCulloh K.A., Woodruff D.R. (2009) Xylem hydraulic safety margins in woody plants: coordination of stomatal control of xylem tension with hydraulic capacitance. *Functional Ecology*, **23**, 922–930.

Mrad A., Johnson D.M., Love D.M., Domec J.C. (2021) The roles of conduit redundancy and connectivity in xylem hydraulic functions. *New Phytologist*, **231**, 996–1007.

Nolan R.H., Gauthey A., Losso A., Medlyn B.E., Smith R., Chhajed S.S., Fuller K., Song M., Li X., Beaumont L.J., Boer M.M., Wright I.J., Choat B. (2021) Hydraulic failure and tree size linked with canopy die-back in eucalypt forest during extreme drought. *New Phytologist*, **230**, 1354–1365.

Oliveira R.S., Costa F.R.C., Baalen E., Jonge A., Bittencourt P.R., Almanza Y., Barros F.D.V., Cordoba E.C., Fagundes M.V., Garcia S., Guimaraes Z., Hertel M., Schietti J., Rodrigues-Souza J., Poorter L. (2019) Embolism resistance drives the distribution of Amazonian rainforest tree species along hydro-topographic gradients. *New Phytologist*, **221**, 1457–1465.

Oliveira R.S., Eller C.B., Barros F.D.V., Hirota M., Brum M., Bittencourt P. (2021) Linking plant hydraulics and the fast–slow continuum to understand resilience to drought in tropical ecosystems. *New Phytologist*, **230**, 904–923.

Olson M.E., Rosell J.A. (2013) Vessel diameter–stem diameter scaling across woody angiosperms and the ecological causes of xylem vessel diameter variation. *New Phytologist*, **197**, 1204–1213.

Pammenter N.V., Van der Willigen C. (1998) A mathematical and statistical analysis of the curves illustrating vulnerability of xylem to cavitation. *Tree Physiology*, **18**, 589–593.

Pan R., Geng J., Cai J., Tyree M.T. (2015) A comparison of two methods for measuring vessel length in woody plants. *Plant, Cell & Environment*, **38**, 2519–2526.

Paulo A.A., Rosa R.D., Pereira L.S. (2012) Climate trends and behaviour of drought indices based on precipitation and evapotranspiration in Portugal. *Natural Hazards and Earth System Sciences*, **12**, 1481–1491.

Pereira L., Miranda M.T., Pires G.S., Pacheco V.S., Guan X., Kaack L., Karimi Z., Machado E.C., Jansen S., Tyree M.T., Ribeiro R.V. (2020) A semi-automated method for measuring xylem vessel length distribution. *Theoretical and Experimental Plant Physiology*, **32**, 331–340.

Pivovaroff A.L., Sack L., Santiago L.S. (2014) Coordination of stem and leaf hydraulic conductance in southern California shrubs: a test of the hydraulic segmentation hypothesis. *New Phytologist*, **203**, 842–850.

Powers J.S., Vargas G. G., Brodribb T.J., Schwartz N.B., Pérez-Aviles D., Smith-Martin C.M., Becknell J.M., Aureli F., Blanco R., Calderón-Morales E., Calvo-Alvarado J.C., Calvo-Obando A.J., Chavarría M.M., Carvajal-Vanegas D., Jiménez-Rodríguez C.D., Murillo Chacon E., Schaffner C.M., Werden L.K., Xu X., Medvigy D. (2020) A catastrophic tropical drought kills hydraulically vulnerable tree species. *Global Change Biology*, **26**, 3122–3133.

Rodriguez-Dominguez C.M., Brodribb T.J. (2020) Declining root water transport drives stomatal closure in olive under moderate water stress. *New Phytologist*, **225**, 126–134.

Rodriguez-Dominguez C.M., Carins Murphy M.R., Lucani C., Brodribb T.J. (2018) Mapping xylem failure in disparate organs of whole plants reveals extreme resistance in olive roots. *New Phytologist*, **218**, 1025–1035.

Schenk H.J., Jansen S., Hölttä T. (2021) Positive pressure in xylem and its role in hydraulic function. *New Phytologist*, **230**, 27–45.

Schindelin J., Arganda-Carreras I., Frise E., Kaynig V., Longair M., Pietzsch T., Preibisch S., Rueden C., Saalfeld S., Schmid B., Tinevez J.-Y., White D.J., Hartenstein V., Eliceiri K., Tomancak P., Cardona A. (2012) Fiji: an open-source platform for biological-image analysis. *Nature Methods*, **9**, 676–682.

Schuldt B., Buras A., Arend M., Vitasse Y., Beierkuhnlein C., Damm A., Gharun M., Grams T.E.E., Hauck M., Hajek P., Hartmann H., Hiltbrunner E., Hoch G., Holloway-Phillips M., Körner C., Larysch E., Lübbe T., Nelson D.B., Rammig A., Rigling A., Rose L., Ruehr N.K., Schumann K., Weiser F., Werner C., Wohlgemuth T., Zang C.S., Kahmen A. (2020) A first assessment of the impact of the extreme 2018 summer drought on Central European forests. *Basic and Applied Ecology*, **45**, 86–103.

Schuldt B., Knutzen F., Delzon S., Jansen S., Müller-Haubold H., Burlett R., Clough Y., Leuschner C. (2016) How adaptable is the hydraulic system of European beech in the face of climate change-related precipitation reduction? *New Phytologist*, **210**, 443–458.

Scoffoni C., Albuquerque C., Brodersen C.R., Townes S.V., John G.P., Cochard H., Buckley T.N., McElrone A.J., Sack L. (2017) Leaf vein xylem conduit diameter influences susceptibility to embolism and hydraulic decline. *New Phytologist*, **213**, 1076–1092.

Sergent A.S., Varela S.A., Barigah T.S., Badel E., Cochard H., Dalla-Salda G., Delzon S., Fernández M.E., Guillemot J., Gyenge J., Lamarque L.J., Martinez-Meier A., Rozenberg P., Torres-Ruiz J.M., Martin-StPaul N.K. (2020) A comparison of five methods to assess embolism resistance in trees. *Forest Ecology and Management*, **468**, 118175.

Skelton R.P., Dawson T.E., Thompson S.E., Shen Y., Weitz A.P., Ackerly D. (2018) Low vulnerability to xylem embolism in leaves and stems of North American oaks. *Plant Physiology*, **177**, 1066–1077.

Smith-Martin C.M., Skelton R.P., Johnson K.M., Lucani C., Brodribb T.J. (2020) Lack of vulnerability segmentation among woody species in a diverse dry sclerophyll woodland community. *Functional Ecology*, **34**, 777–787.

Sorek Y., Greenstein S., Netzer Y., Shtein I., Jansen S., Hochberg U. (2021) An increase in xylem embolism resistance of grapevine leaves during the growing season is coordinated with stomatal regulation, turgor loss point and intervessel pit membranes. *New Phytologist*, **229**, 1955–1969.

Sperry J.S., Hacke U.G., Wheeler J.K. (2005) Comparative analysis of end wall resistivity in xylem conduits. *Plant, Cell & Environment*, **28**, 456–465.

Sperry J.S., Tyree M.T. (1988) Mechanism of water stress-induced xylem embolism. *Plant Physiology*, **88**, 581–587.

Torres-Ruiz J.M., Cochard H., Choat B., Jansen S., López R., Tomášková I., Padilla-Díaz C.M., Badel E., Burlett R., King A., Lenoir N., Martin-StPaul N.K., Delzon S. (2017) Xylem resistance to embolism: presenting a simple diagnostic test for the open vessel artefact. *New Phytologist*, **215**, 489–499.

Torres-Ruiz J.M., Jansen S., Choat B., McElrone A.J., Cochard H., Brodribb T.J., Badel E., Burlett R., Bouche P.S., Brodersen C.R., Li S., Morris H., Delzon S. (2015) Direct X-ray microtomography observation confirms the induction of embolism upon xylem cutting under tension. *Plant Physiology*, **167**, 40–43.

Tyree M.T. (1988) A dynamic model for water flow in a single tree: evidence that models must account for hydraulic architecture. *Tree Physiology*, **4**, 195–217.

Tyree M.T., Ewers F.W. (1991) The hydraulic architecture of trees and other woody plants. *New Phytologist*, **119**, 345–360.

Tyree M.T., Sperry J.S. (1989) Vulnerability of xylem to cavitation and embolism. *Annual Review of Plant Biology*, **40**, 19–36.

Vandeleur R.K., Mayo G., Shelden M.C., Gilliham M., Kaiser B.N., Tyerman S.D. (2009) The role of plasma membrane intrinsic protein aquaporins in water transport through roots: diurnal and drought stress responses reveal different strategies between isohydric and anisohydric cultivars of grapevine. *Plant Physiology*, **149**, 445–460.

Wang Y., Burlett R., Feng F., Tyree M. (2014) Improved precision of hydraulic conductance measurements using a Cochard rotor in two different centrifuges. *Journal of Plant Hydraulics*, **1**, e0007.

Wason J.W., Anstreicher K.S., Stephansky N., Huggett B.A., Brodersen C.R. (2018) Hydraulic safety margins and air-seeding thresholds in roots, trunks, branches and petioles of four northern hardwood trees. *New Phytologist*, **219**, 77–88.

Wason J., Bouda M., Lee E.F., McElrone A.J., Phillips R.J., Shackel K.A., Matthews M.A., Brodersen C. (2021) Xylem network connectivity and embolism spread in grapevine (*Vitis vinifera* L.). *Plant Physiology*, **186**, 373–387.

Wheeler J.K., Huggett B.A., Tofte A.N., Rockwell F.E., Holbrook N.M. (2013) Cutting xylem under tension or supersaturated with gas can generate PLC and the appearance of rapid recovery from embolism. *Plant, Cell & Environment*, **36**, 1938–1949.

Wheeler J.K., Sperry J.S., Hacke U.G., Hoang N. (2005) Inter-vessel pitting and cavitation in woody Rosaceae and other vesselled plants: a basis for a safety versus efficiency trade-off in xylem transport. *Plant, Cell & Environment*, **28**, 800–812.

Yan C.L., Ni M.Y., Cao K.F., Zhu S.D. (2020) Leaf hydraulic safety margin and safety–efficiency trade-

off across angiosperm woody species. *Biology Letters*, **16**, 20200456.

Zhang Q.W., Zhu S.D., Jansen S., Cao K.F. (2021) Topography strongly affects drought stress and xylem embolism resistance in woody plants from a karst forest in Southwest China. *Functional Ecology*, **35**, 566–577.

Zhang Y.A., Carmesin C., Kaack L., Klepsch M.M., Kotowska M., Matei T., Schenk H.J., Weber M., Walther P., Schmidt V., Jansen S. (2020) High porosity with tiny pore constrictions and unbending pathways characterize the 3D structure of intervessel pit membranes in angiosperm xylem. *Plant, Cell & Environment*, **43**, 116–130.

Zhang Y.A., Lamarque L.J., Torres-Ruiz J.M., Schuldt B., Karimi Z., Li S., Qin D.-W., Bittencourt P., Burlett R., Cao K.-F., Delzon S., Oliveira R., Pereira L., Jansen S. (2018) Testing the plant pneumatic method to estimate xylem embolism resistance in stems of temperate trees. *Tree Physiology*, **38**, 1016–1025.

Zhu S.D., Li R.H., He P.C., Siddiq Z., Cao K.F., Ye Q. (2019) Large branch and leaf hydraulic safety margins in subtropical evergreen broadleaved forest. *Tree Physiology*, **39**, 1405–1415.

Zhu S.D., Liu H., Xu Q.Y., Cao K.F., Ye Q. (2016) Are leaves more vulnerable to cavitation than branches? *Functional Ecology*, **30**, 1740–1744.

Zhu S.D., Song J.J., Li R.H., Ye Q. (2013) Plant hydraulics and photosynthesis of 34 woody species from different successional stages of subtropical forests. *Plant, Cell & Environment*, **36**, 879–891.

Ziegler C., Coste S., Stahl C., Delzon S., Levionnois S., Cazal J., Cochard H., Esquivel-Muelbert A., Goret J.-Y., Heuret P., Jaouen G., Santiago L.S., Bonal D. (2019) Large hydraulic safety margins protect Neotropical canopy rainforest tree species against hydraulic failure during drought. *Annals of Forest Science*, **76**, 115.

Zimmermann M.H. (1983) *Xylem structure and the ascent of sap*. Springer, Berlin, Germany.